File ID	uvapub:3753
Filename	32226y.pdf
Version	unknown

SOURCE (OR PART OF THE FOLLOWING SOURCE):

Type	article
Title	Detection of pulsed X-ray emission from the binary millisecond pulsar PSR J0218+4232
Author(s)	L. Kuiper, W. Hermsen, F. Verbunt, T. Belloni
Faculty	FNWI: Astronomical Institute Anton Pannekoek (IAP)
Year	1998

FULL BIBLIOGRAPHIC DETAILS:
   http://hdl.handle.net/11245/1.140479

ASTRONOMY
AND
ASTROPHYSICS

Detection of pulsed X-ray emission
from the binary millisecond pulsar PSR J0218+4232

L. Kuiper[1], **W. Hermsen**[1], **F. Verbunt**[2], **and T. Belloni**[3]

[1] SRON-Utrecht, Sorbonnelaan 2, 3584 CA Utrecht, The Netherlands
[2] Astronomical Institute, Utrecht University, P.O. Box 80000, 3508 TA Utrecht, The Netherlands
[3] Astronomical Institute Anton Pannekoek and Center for High-Energy Astrophysics, Kruislaan 403, 1098 SJ Amsterdam, The Netherlands

Abstract. We report the detection of pulsed X-ray emission from the binary millisecond pulsar PSR J0218+4232 in a 100 ks ROSAT HRI observation. The lightcurve deviates from a flat distribution at a $\sim 4.8\sigma$ level, showing a sharp main pulse with a duty cycle of $\sim 0.15\,(350\mu s)$, compatible with smearing due to the scatter in the ROSAT clock calibration. The intrinsic width can be smaller than $100\mu s$. There is an indication for a second peak at a phase separation of 0.47 ± 0.01. The pulsed fraction is $37 \pm 13\%$. No indication for a modulation at the orbital period of the binary system is found. This is the fourth millisecond pulsar showing modulation in X-rays at the radio-pulsar period. The sharp pulses, very similar to those of PSR B1821-24 and the Crab pulsar, point to a magnetospheric origin of the pulsed X-ray emission. The observed and derived parameters of PSR J0218+4232 and PSR B1821-24 are very consistent with the exception of the small pulsed fraction of PSR J0218+4232. The large unpulsed component in X-rays and that reported earlier in the radio domain can be explained by emission from a compact nebula with diameter $\sim 14''$.

Key words: pulsars: individual: PSR J0218+4232; PSR B1821-24 – stars: neutron – X-rays: stars

1. Introduction

PSR J0218+4232 was discovered by Navarro et al. (1995) as a highly luminous 2.3 ms radio-pulsar in a 2.0 day orbit. This milli-second (ms) pulsar has an extremely broad pulse-profile and about half of the radio emission is unpulsed; this is taken by Navarro et al. (1995) as an indication that the magnetic field is almost aligned with the rotation axis. From the dispersion measure a lower limit on the distance of 5.7 kpc is derived.

Van Kerkwijk (1997) reported the detection of an optical counterpart for this recycled ms-pulsar. The pulsar mass function as given by Navarro et al. (1995) suggests a companion mass of $\sim 0.2 M_{\odot}$.

Recently, Verbunt et al. (1996) detected soft X-ray emission from this source in a 22 ksec ROSAT HRI observation. A timing analysis yielded a 6% probability that the observed phase

distribution was due to random processes. They also found indications for pulsed emission in an archival ROSAT PSPC observation with the pulsar at an unfavourable off-axis angle of $40'$. The significance for pulsed emission ranged from 2.5σ to 4σ depending on the size of the event extraction radius. Verbunt et al. (1996) conservatively reported a value of 2.5σ since the usage of an extraction radius is in this case not an optimum selection criterion in view of the "horse-shoe" - shaped far off-axis PSPC point spread function. Therefore the detection of pulsed emission was considered tentative. The ROSAT HRI and PSPC lightcurves suggested a double-peaked lightcurve.

Pulsed X-ray emission has been firmly detected sofar from only 3 ms-pulsars, namely PSR J0437-4715 (Becker & Trümper 1993), PSR B1821-24 (Saito et al. 1997) and PSR J2124-3358 (Becker & Trümper 1997).

It was also noticed by Verbunt et al. (1996) that the EGRET high-energy γ-ray source 2EG J0220+4228 (Thompson et al. 1995), detected above 100 MeV at a $> 5\sigma$ significance is positionally consistent with the pulsar. A timing analysis using archival EGRET > 100 MeV data yielded indications for pulsed emission above 100 MeV at significance levels slightly below 3σ, making 2EG J0220+4228 a potential high-energy gamma-ray counterpart for PSR J0218+4232.

In this paper the results are presented from a 100 ks follow-up observation of PSR J0218+4232 with the ROSAT XRT/HRI combination aimed at clarifying its soft X-ray (0.1-2.4 keV) timing properties.

2. X-ray data and data analysis

2.1. ROSAT HRI observation

PSR J0218+4232 was observed nearly on-axis with the ROSAT XRT/HRI combination between 23 July 1997 and 31 July 1997 yielding a net exposure of 98069 s. A standard analysis of the HRI image confirmed the detection by Verbunt et al. (1996) of a source consistent in position with the radio-pulsar. The measured offset of $4''\!.2$ is smaller than the systematic uncertainty in the satellite pointing of $6''\!.0$. Fig. 1 shows the measured event distribution and the position of the radio-pulsar without boresight correction.
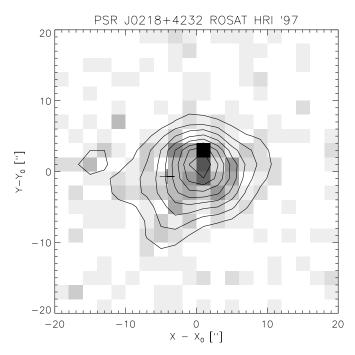
Fig. 1. Measured (x,y)-distribution (in $2\farcs0 \times 2\farcs0$ pixels) centered on the position of the X-ray counterpart of PSR J0218+4232. The position of the pulsar, indicated by a '+' sign, is consistent with the position of the X-ray source which has a systematic uncertainty of $\sim 6\farcs0$. Superposed is the smoothed distribution (equidistant contour levels) obtained after convolving the measured distribution with a 2-dimensional Gaussian with $\sigma = 2\farcs0$, approximately the width of the point-spread function derived from ground-based calibrations and in-flight measurements (David et al. 1997). The highest pixel contains 14 counts.

2.2. Spatial analysis

The standard analysis was applied to determine the centroid of the source event distribution using a Gaussian shaped Point Spread Function (PSF) with a predetermined standard deviation (Zimmermann et al. 1997). However, the in-flight PSF could have a somewhat different shape and width. In addition, we have to verify whether the source distribution is consistent with a single point source. To derive this in-flight distribution we have determined the radial distribution with respect to the centroid (r=0) of the number of events per arcsec square. This distribution is shown in Fig. 2a. For radii beyond $20\farcs0$ the background level is evidently reached. We found for the latter a value of (0.093 ± 0.004) cnts/arcsec^2 by chosing the background region between r is $20\farcs0$ and $50\farcs0$. By subtracting this underlying background contribution from the measured (including both source and background events) radial distribution we can determine the cumulative radial distribution of the source events. This distribution saturates at a value of ~ 182 cnts, corresponding to the total number of source counts, and its shape is compatible with a Gaussian having a standard deviation of $4\farcs75$ (see Fig. 2b; empirically derived source distribution).

This value is larger than expected from the on-axis PSF derived from ground-based calibrations and in-flight observations (David et al. 1997). The latter is described as the sum of

two Gaussians and an exponential and gives on average a good representation. Due to random errors in the aspect solution of the spacecraft, the width of the core of the measured response can vary. David et al. (1997) give a range for the widths of the Gaussian components as derived from in-flight observations. In Figs. 2a,b the expected profiles are shown for comparison ($\sigma_1 = 2\farcs19$ and $\sigma_2 = 4\farcs04$; see David et al. 1997). It is evident that the measured profile is significantly broader than that expected for a point source. This can be due to the detection of a point source plus extended emission, unless systematic effects have broadened the profile excessively. We will investigate these possibilities below.

In order to derive a measure for the overall significance and flux of the total excess, we repeated the spatial analysis by applying a maximum likelihood ratio test using the empirically derived source distribution. This maximum likelihood ratio test is based on parameter optimization under two different hypotheses, one describing the measured (x,y) - event distribution by background only ($\mathcal{H}_0$) and the alternative ($\mathcal{H}_1$) describing the event distribution by background and a point source (the empirical source distribution) at a given scan position. This test yielded a 21σ source detection. The number of counts S assigned to the total excess and background B per arcsec square is (181.4 ± 15.0) cnts and (0.094 ± 0.004) cnts/arcsec^2, respectively, fully consistent with the above estimates. The countrate is $(1.84 \pm 0.15) \cdot 10^{-3}$ cnts/s, which is consistent with the value of $(2.1 \pm 0.4) \cdot 10^{-3}$ cnts/s from our previous 22 ks ROSAT/HRI observation (Verbunt et al. 1996).

Having decoupled the source and background distributions we were able to determine the Signal-to-Noise ratio ($S/N = (Q(r) - \pi \cdot B \cdot r^2)/\sqrt{Q(r)}$) as a function of distance r from the centroid (Fig. 2c). The quantity $Q(r)$ represents the measured cumulative count distribution as function of distance r including both source and background events. The optimum radius $r_{opt} = 11\farcs25$ is used as *extraction* radius in the subsequent timing analyses.

2.3. Timing analyses

2.3.1. Modulation at the pulsar period

In the search for modulation at the pulsar period we selected events within a radius r_{opt}, the optimum radius determined above, from the X-ray source position. The solar-system barycentered (SSB) UTC arrival times were converted to barycentric dynamical time scale (TDB). These SSB UTC arrival times in turn were obtained by converting the space-craft clock (SCC) arrival times to UTC times using a fourth order polynomial fit of the SCC-calibration points to UTC, and subsequently determining the source -, space-craft - and SSB position dependent parts. Because our observation was spread over more than 8 days the stability of the SCC - UTC fit over the observation period is crucial for a successfull modulation search at *millisecond* periods. We have been fortunate, the average scatter around the mean of the fit residuals over the entire observation was in an acceptable range ($\lesssim 0.20$ ms, correspond-
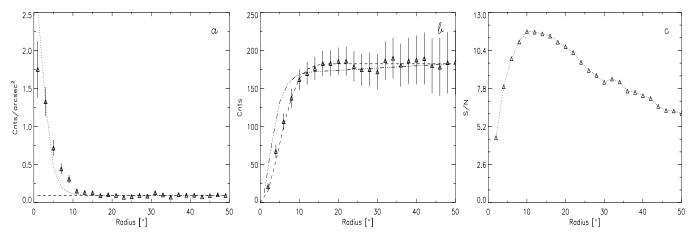
Fig. 2. a Radial distribution of the surface density centered on the X-ray counterpart of PSR J0218+4232. The dashed line indicates the background level determined from the distribution for radii between $20\rlap{.}''0$ and $50\rlap{.}''0$. The dotted line shows the expected profile for a point source (David et al. 1997). **b** Cumulative background- subtracted distribution for the X-ray counterpart of PSR J0218+4232. The dashed line shows the distribution for a Gaussian shaped source distribution with $\sigma = 4\rlap{.}''75$ and 182 source counts. The dashed-dotted line shows the expected cumulative distribution for a point source having 182 counts. **c** The Signal-to-Noise distribution as a function of the event extraction radius r. This distribution peaks at $r = r_{opt} = 11\rlap{.}''25$, the optimum extraction radius for timing studies.
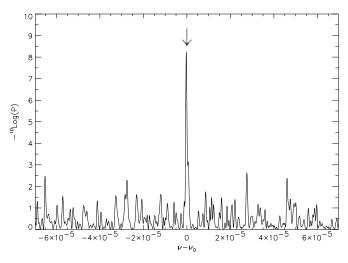

Fig. 3. Periodogram for our HRI'97 observation at frequencies in the vicinity of the expected radio-pulse frequency ν_0. Along the y-axis is shown the chance probability from the Z_2^2-test. The expected frequency (downwards arrow) falls within the measured peak with a characteristic width $\Delta\nu$ of $\sim 1/\tau = 1.4 \cdot 10^{-6}$ Hz with τ the total observation interval ($8\rlap{.}^{\mathrm{d}}3$).

ing to a scatter in pulse-phase of $\lesssim 0.1$). (see e.g. ROSAT Service Area; chapter on Calibration sub. Timing; http://ftp.rosat.mpe-garching.mpg.de/rosat_svc/calibration/timing/). The next step in our analysis was pulse-phase folding the TDB-arrival times according to the radio ephemeris given by Navarro et al. (1995) taking into account the time-delays due to the orbital motion. We verified that the uncertainty in the predicted period is sufficiently small to justify a single trial at the expected radio parameters.

The obtained pulse-phase distribution deviates from a statistically flat distribution at a $\sim 4.8\sigma$ level (chance probability of $1.96 \cdot 10^{-6}$) for two harmonics ($n = 2$) applying a Z_n^2- test (see Buccheri et al. 1983) on the unbinned set of pulse-

phases. An H-test (de Jager et al. 1989), also on the unbinned set of pulse-phases and more appropriate if the pulse-shape is unknown, yields a chance probability of $1.94 \cdot 10^{-5}$ corresponding to a $\sim 4.4\sigma$ deviation. We verified the association of the pulsed emission with the pulsar by performing a similar timing analysis but now selecting events having radii larger than r_{opt}. No modulation is present in this sample. Furthermore, the periodogram in Fig. 3 shows that the detected pulsar modulation is only visible around the expected frequency $\nu_0 = 430.461066552(7)$ Hz with a width $\Delta\nu$ consistent with the total observation interval.

The lightcurve (binned representation of the pulse-phase distribution) obtained after phase-folding at the expected radio frequency (single trial) is shown in Fig. 4 for two cycli with superimposed its Kernel Density Estimator (de Jager 1986; solid smooth line) and its 1σ-uncertainty range (dashed-dotted lines). The phase in Fig. 4 is arbitrary, for we can not relate the X-ray phase to the radio-phase due to the limited accuracy of the ROSAT timing. Indicated as a dashed line is the background level determined from the spatial analysis. It is evident that a considerable fraction of the source photons is unpulsed (DC). In order to quantify the pulsed fraction we have applied a method based on bootstrapping of the (unbinned) data to determine the strength of the pulsed signal and the unpulsed interval in an unbiased manner as outlined in Swanepoel et al. (1996). This method assigns the pulse-phase interval $[0.12 - 0.39]$ as the unpulsed interval (statistically flat) and the pulsed fraction $\mathcal{R} = N_P/(N_P + N_{DC})$ obtained by this recipe is 0.37 ± 0.13, where N_P and N_{DC} are the number of pulsed and DC counts, respectively.

The dominant emission feature above the DC-flux level (in phase range 0.45-0.60) has a remarkably small duty cycle of ~ 0.15 ($350\mu s$) which is compatible with the effect of smearing due to the scatter in the SCC - UTC clock calibration (see above). The intrinsic width can be significantly less than $100\mu s$.
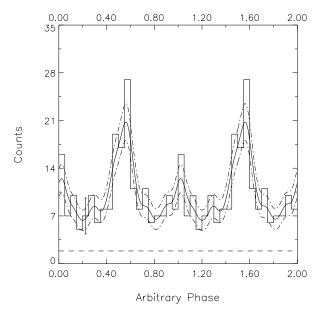
Fig. 4. Lightcurve for the 100 ks ROSAT HRI 1997 observation of PSR J0218+4232. Two cycles are shown for clarity. A typical error bar is shown. The significance for a deviation from a statistically flat distribution is $\sim 4.8\sigma$. The dashed line indicates the background level determined from the spatial analysis. The pulsed fraction is estimated to be $(37 \pm 13\%)$. The smooth solid curve represents the Kernel Density Estimator and the dashed-dotted lines indicate the 1σ uncertainty range.

Fig. 5. Co-added HRI'97, HRI'95 and PSPC lightcurve obtained after applying the phase-shifts at cross-correlation maxima (see text). A typical error bar is indicated. The dashed line represents the level of unpulsed emission determined in the phase range [0.12-0.39]. The features visible in Fig. 4 become more pronounced. The second peak (phase range [−0.12-0.12]) contains 50 ± 14 excess counts corresponding to a $\sim 3.6\sigma$ detection.

There appears to be a second pulse (near 1.0 in phase), although it is marginally significant in this 100 ks ROSAT HRI observation: the improvement in likelihood of a pulse-phase distribution description in terms of a background and 2 Gaussians with respect to a description in terms of a background and 1 Gaussian corresponds to 1.6σ. The 2 Gaussians have a phase separation of 0.47 ± 0.01. Our earlier HRI and PSPC lightcurves suggested also two pulses (Verbunt et al. 1996). Unfortunately, all lightcurves have arbitrary phase, so we can not directly sum the distributions. To derive the phase shifts from the lightcurves we cross-correlated the ROSAT/HRI 1995 and ROSAT/PSPC lightcurves with the ROSAT/HRI 1997 lightcurve and select the global maxima. Applying these shifts we obtain the co-added lightcurve shown in Fig. 5. It is remarkable to see how this combined lightcurve strengthens the features visible in Fig. 4 : The main pulse becomes more significant with a similar or smaller pulse width; the second pulse becomes also more pronounced with similar width; the phase separation is again 0.47 ; and the background region identified by the bootstrapping method in the lightcurve of the HRI 1997 observation represents even more clearly the unpulsed level. This level is drawn in Fig. 5 as a dashed-dotted line adopting the unpulsed interval [0.12 − 0.39] as determined above. The number of counts in the second peak (phase range [−0.12, 0.12]) above the unpulsed level is $50 \pm 14 \, (\sim 3.6\sigma)$ giving additional support for the presence of a second peak. In fact, this phase distribution mimics the well-known X-ray lightcurve of the Crab pulsar which exhibits also two peaks with phase separation 0.40 and emission between the peaks.
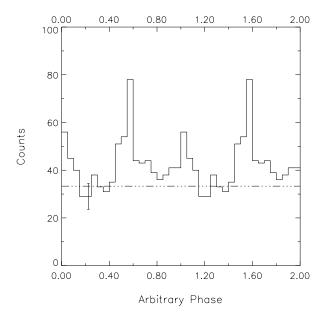
2.3.2. Modulation at the orbital period

We also searched for a possible modulation at the binary period of $2\overset{d}{.}0288$. In this case we have to divide the number of counts detected within r_{opt} per orbital phase bin by its exposure to obtain the countrate corrected for the inhomogeneous exposure. Dividing the orbital cycle in 10 and 20 bins we found no indication for orbital modulation ($\chi_r^2 = 1.05$ and $\chi_r^2 = 1.12$, respectively, fitting a constant countrate). An X-ray eclipse could be expected near $\phi_{orb} = 0.25$ ($\phi_{orb} = 0$ corresponds to the time of the ascending node). The flux measurement around this phase does not show any suppression.

2.4. Indications for extended emission

In Sect. 2.2 we concluded from Fig. 2a,b that the excess in the skymap has an extent which is larger than expected for a point source based on ground-based calibrations and in-flight observations (David et al. 1997). The detection of a pulsed signal in the timing analysis with a pulsed fraction of $37 \pm 13\%$ proves that at least a significant fraction originates in a point source. For the remaining unpulsed component of $\sim 63\%$ there are two explanations possible: 1) Point-like emission from the pulsar, but then the PSF of the pulsed and unpulsed emission would be excessively broadened by systematic effects; 2) extended emission.

In order to investigate these possibilities, we produced a "pulsed" map selecting events in the pulse-phase interval of the main pulse (phase range 0.45-0.60; see Fig. 4) and an "unpulsed"
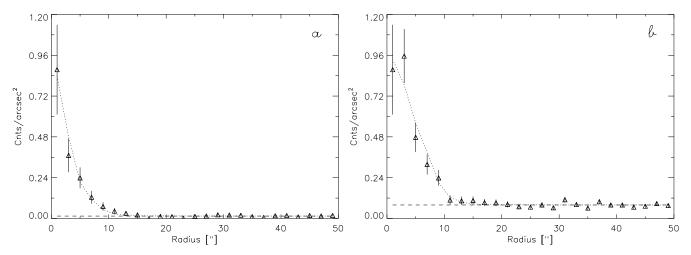
Fig. 6. a Radial event distribution of the X-ray counterpart of PSR J0218+4232 selecting events with pulse-phases in the range 0.45-0.60 (main peak). The dotted line shows the distribution expected from a point-source with weight factor 0.7 and an extended model (cylinder model with radius $7''.0$) with weight factor 0.3. **b** Radial event distribution of the X-ray counterpart of PSR J0218+4232 selecting events with pulse-phases in range 0.0-0.45 and 0.60-1.0. The dotted line shows the distribution expected from a point-source with weight factor 0.13 and the extended model with weight factor 0.87. Note the sharper shape of the radial distribution of the main peak shown in **a** in comparison with the shape of the complementary distribution shown in **b**.

map for the complementary phase range (0.0-0.45 and 0.6-1.0). If systematic effects are not responsible for the broad total profile, then the profile in the pulsed map should be narrower, because in that case we selected an event sample with a pulsed fraction of $70 \pm 6\%$. This pulsed fraction has been determined from the number of excess counts in the main peak above the level in the unpulsed phase interval 0.12-0.39 (see Sect. 2.3.1; bootstrap method as outlined in Swanepoel et al. 1996). Note that the pulsed fraction in the complementary phase interval is also non-zero: $13 \pm 11\%$.

Fig. 6 displays for the pulsed and unpulsed maps the differential radial profiles analogous to Fig. 2a for the total data. Indeed, the distribution in the pulsed map (Fig. 6a) is sharper, only slightly broader than expected for a point source. In order to investigate this more quantitatively, we compared the measured distributions with the expected profile for the (weighted) sum of two components: A point source plus an extended distribution, assumed to have the shape of a cylinder. The latter distribution has been convolved with the expected PSF for a point source (David et al. 1997).

To derive an estimate of the diameter of the extended emission, we made a fit to the total radial profile (Fig. 2a) in terms of a point source with a *fixed* contribution of 37% and an extended model (63%) yielding for the diameter of the extended emission a 1σ-confidence interval of $[12'' - 15'']$ with an optimum value near $14''$.

Figs. 6a and b show that also these distributions are fully consistent with the sums of the expected profiles for a point source (weight factors 0.70 and 0.13, respectively) and extended emission with diameter $14''$ (weight factors 0.30 and 0.87, respectively). The obtained reduced χ^2-values were 0.58 and 0.85, respectively, both for 5 degrees of freedom (d.o.f.; the effective fit range was $0''.0 < r < 12''.0$, which includes 6 datapoints). In order to quantify the differences between the distributions we

have also fit the radial distribution of the pulsed events in Fig. 6a with the profile used in the fit of the complementary distribution in Fig. 6b. The reduced χ^2 was then 2.21, again for 5 d.o.f. The chance probability for such a large value of the reduced χ^2 is $\sim 5\%$, indicating that the fit is rejectable at the 95%- confidence level.

Finally, we also investigated whether the weight of the point source can be increased fitting again the total radial profile (Fig. 2a), leaving both the radius of the extended emission and the point source fraction free, to see how much DC emission from the point source is allowed in addition to the extended emission. We do not find a significant detection, the 1σ-confidence interval for the *total* point source fraction being [0.2-0.65] to be compared with that for the pulsed fraction from the timing analysis [0.24-0.50].

An independent method to study the extent of the in-flight PSF consists in identifying point-sources with high photon statistics in the vicinity (within $\sim 10'$) of PSR J0218+4232 and subsequently analyzing their radial profiles. We only found 3 weak sources, all weaker than PSR J0218+4232 and therefore less appropriate for this kind of study. None of these show the same broadening as PSR J0218+4232.

From the above findings we can conclude that we found indications for extended emission with an angular scale of $\sim 14''$, centered on the pulsar position.

2.5. Flux calculation

The ROSAT HRI has no spectral resolving power, making spectral modelling impossible. However, assuming a spectral model and a measure of the Hydrogen column density (N_H) in the direction of the source, it is possible to convert the total measured countrate to an unabsorbed flux value (David et al. 1997). For a power-law photon spectrum as found for peak

1 of PSR B1821+24 (Saito et al. 1997) with photon-index $\Gamma = -1.5$ between $0.7 - 10\ keV$ (energy index α is -0.5) and $N_H = 5 \cdot 10^{20}\ \mathrm{cm}^{-2}$ (see Verbunt et al. 1996) the observed countrate translates in an unabsorbed 0.1-2.4 keV flux of $(1.05 \pm 0.09) \cdot 10^{-13}\ \mathrm{ergs/cm}^2\mathrm{s}$. Varying the power-law photon index from -1.0 to -3.0 we obtain flux values between $0.97 \cdot 10^{-13}$ and $2.96 \cdot 10^{-13}\ \mathrm{ergs/cm}^2\mathrm{s}$. Varying also N_H to a value of $7.5 \cdot 10^{20}\ cm^{-2}$ found from the H I-survey performed by Heiles & Habing (1974), increases the fluxes by 8 to 24% for power-law indices ranging from -1.0 to -3.0, respectively. Assuming, a fortiori, that the pulsed and unpulsed components have the same spectral shape, we can divide the total flux of $(1.05 \pm 0.09) \cdot 10^{-13}\ \mathrm{ergs/cm}^2\mathrm{s}$ for $N_H = 5 \cdot 10^{20}\ cm^2$, $\Gamma = -1.5$ and a pulsed fraction of 37±13% in a pulsed component of $(3.9 \pm 1.4) \cdot 10^{-14}\ \mathrm{ergs/cm}^2\mathrm{s}$ and an unpulsed/extended component of $(6.6 \pm 1.5) \cdot 10^{-14}\ \mathrm{ergs/cm}^2\mathrm{s}$.

3. Discussion

The detection of pulsed X-ray emission from PSR J0218+4232 makes this the fourth ms-pulsar for which modulation at the pulse-period is observed. Of the three other ms-pulsars showing spin-modulated X-ray emission, namely PSR J0437-4715 (Becker & Trümper 1993; Halpern et al. 1996; Kawai et al. 1998), PSR B1821+24 (Danner et al. 1994, 1997; Saito et al. 1997; Rots et al. 1998; Becker & Trümper 1997) and PSR J2124-3358 (Becker & Trümper 1997), only PSR B1821-24 shows narrow pulses in its lightcurve similar to PSR J0218+4232. The other two ms-pulsars, PSR J0437-4715 and PSR J2124-3358, show both broad and smooth X-ray lightcurves. In addition, the latter have luminosities in the ROSAT 0.1-2.4 keV band about 3 orders of magnitude lower than the first two. Therefore we concentrate in the remainder of the discussion on the comparison of PSR J0218+4232 with PSR B1821-24, which have the smallest characteristic ages ($\tau_c = P/2\dot{P}$), by 1-2 orders of magnitude, of the ms-pulsars detected at X-rays sofar.

PSR B1821-24 has been studied in detail by Saito et al. (1997) using ASCA data. They showed that the narrow ($\sim 100\mu$s) first pulse after subtraction of the DC-component has a very hard spectrum (photon index -1.2 between 0.7 and 10 keV), which has to be of magnetospheric origin. Interestingly, the phase separation 0.444 ± 0.014 or alternatively 0.556 (Rots et al. 1998) between the two pulses of PSR B1821-24 is very similar to the 0.47 ± 0.01 measured by us for PSR J0218+4232. In addition, the first pulse in the lightcurve of Figs. 4 and 5 can be intrinsically be narrower than 1 bin, which is also $\sim 100\mu$s. Unfortunately, we cannot derive spectra from our ROSAT HRI observation, but the narrow pulses detected from PSR J0218+4232 make us belief that these are also of magnetospheric origin. The origin of the substantial unpulsed component (see Fig. 4) is less obvious. This could be thermal emission from the neutron star surface as well as of magnetospheric origin. However, this unpulsed component can also be assigned to extended emission from e.g. a compact nebula, as is shown in Sect. 2.4. This will be discussed below.

Most striking are the differences in the shapes of the radio pulses of the two ms-pulsars. Backer & Sallmen (1997) show for PSR B1821-24 two narrow pulses and one broader radio pulse (at 800 and 1395 MHz), very different from the extremely broad radio pulse of PSR J0218+4232 detected throughout the pulsar period (Fig. 7). As mentioned in the introduction, the broad radio-pulse from PSR J0218+4232 was explained with the geometry of an aligned rotator (Navarro et al. 1995), but the two narrow peaks with the indication of bridge emission between them as seen in the X-ray lightcurve (see Figs. 4,5), require at least a small angle between the magnetic - and rotation axis. Namely: Such double-peaked pulses with bridge emission are currently explained by models in which the high-energy emission is seen from one magnetic pole. In polar cap models (most recently: Sturner et al. 1995; Daugherty & Harding 1996) the non-thermal beam is a hollow cone centered on the magnetic pole. In outer gap models (most recently Romani 1996) the emission occurs in a wide fan beam that is formed by the surface of the last open field line in the outer magnetosphere. For both models a double-peaked pulse can only be observed when the rotator is not completely aligned and the edge of the cone is visible to the observer twice per rotation. Unfortunately, we cannot compare the radio and X-ray profiles of PSR J0218+4232 in absolute timing, nor is it possible to identify a common pulse for tentative more detailed discussions like has been done for PSR B1821-24 by Backer & Sallmen (1997). Saito et al. (1997) compared the physical parameters of PSR B1821-24 with those of the Crab pulsar to understand the production of hard emission in the magnetosphere of a ms-pulsar for which the magnetic field strength is orders of magnitude weaker than for normal rotational pulsars. They pointed out that in the magnetosphere near the light-cylinder radius (R_L), the radius at which the magnetosphere, if corotating with the neutron star, will have a speed equal to the speed of light, the magnetic field strength ($B_L = B_S \cdot (R_S/R_L)^3$ with B_S and R_S the averaged magnetic field strength at the neutron star surface and the neutron star radius respectively) comes out to be very close to that for the Crab. In addition, R_L of ms-pulsars is 1-2 orders of magnitude smaller than those of the young normal pulsars, increasing strongly the curvature of the magnetic field lines which enhances the production of non-thermal emission (see Ho 1989). With our firm detection of pulsed emission from PSR J0218+4232 with a lightcurve similar to those of the Crab pulsar and the isolated ms-pulsar PSR B1821-24 it is interesting to compare now the physical parameters of the two ms-pulsars in more detail (see Table 1). They have very similar periods, PSR J0218+4232 rotating a bit faster, but PSR B1821-24 is $\sim$15 times younger, has a rotational energy loss $\dot{E}$ $\sim$9 times higher and a surface magnetic field strength B_S $\sim$5 times stronger. This suggests that the X-ray luminosity of PSR B1821-24 will be higher, as is indeed the case. The pulsed X-ray luminosities in the ROSAT band (0.1-2.4 keV) differ at most a factor of $\sim$ 10, proportional to the difference in $\dot{E}$, but the total X-ray luminosities differ at most by a factor of 4.

The derived total radio luminosity of PSR J0218+4232 is about a factor of three higher, while the luminosities of the
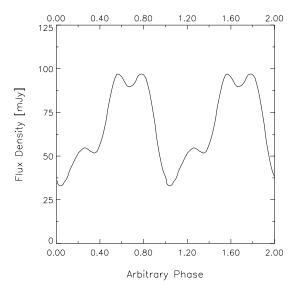
Fig. 7. Radio-profile at 410 MHz of PSR J0218+4232 as shown in Navarro et al. (1995). The pulse shape is broad and complex. Notice that there is no flat baseline to the profile at any phase. The pulsed fraction is about 50%.

Table 1. Parameter comparison between PSR J0218+4232 and PSR B1821-24 (from Navarro et al. 1995, Saito et al. 1997 and this work)

Parameter	J0218+4232	B1821-24
Period (ms)	2.323	3.054
Period derivative (s/s)	$8.00 \cdot 10^{-20}$	$161.88 \cdot 10^{-20}$
Age $P/2\dot{P}$ (yr)	$4.6 \cdot 10^8$	$3.0 \cdot 10^7$
$\dot{E}$ (ergs/s)	$2.5 \cdot 10^{35}$	$2.2 \cdot 10^{36}$
R_L (km)	110.8	145.7
B_S (G)	$4.4 \cdot 10^8$	$2.2 \cdot 10^9$ ♡
B_L (G)	$3.2 \cdot 10^5$	$7.3 \cdot 10^5$
Distance (kpc)	≥ 5.7	5.1♣
L_X (0.1-2.4 keV; ergs/s)		
Total	$\geq 4.1 \cdot 10^{32}$	$1.1^{\dagger}$ -$1.7^{\ddagger} \cdot 10^{33}$
Pulsed	$\geq 1.5 \cdot 10^{32}$	$1.1^{\dagger}$ -$1.7^{\ddagger} \cdot 10^{33}$
L_{Radio} (400 MHz; mJy $\cdot$ kpc^2)		
Total	> 2700	835♠
Pulsed	> 1137	≤ 835

† X-ray luminosity given by Danner et al. (1997)
‡ X-ray luminosity given by Becker & Trümper (1997)
♠ 400 MHz radio luminosity given by Foster et al. (1991) multiplied by $(5.1/5.8)^2$
♣ Rees & Cudworth (1991)
♡ The magnetic field strength at the surface calculated by us is a factor of 2 lower than the value given by Saito et al. (1997). The difference can be traced back to the use of a factor of $\frac{1}{2}$ by Saito et al. in the formula relating the magnetic dipole moment to B_S and R_S. Our factor of 1 is consistent with that widely used in the pulsar community (e.g. Taylor et al. 1993, Becker & Trümper 1997, Navarro et al. 1995).

pulsed radio components are, within the uncertainties on the distance estimates, about the same. It is interesting to note that the magnetic field strength B_L at the light-cylinder of PSR J0218+4232 is only a factor of ~ 2 smaller than that of PSR B1821-24 due to its smaller R_L (~ 110 km vs ~ 146 km). More remarkably, B_L of PSR J0218+4232 is only a factor of ~ 3 smaller than B_L of the Crab pulsar, while B_S differs in this case more than 4 orders of magnitude (see also Saito et al. 1997).

The main difference in characteristics is the remarkably large fraction of unpulsed emission of $\sim$60% in X-rays (see Fig. 4) and $\sim$50% in radio (see Fig.7; systematically over the range 400–1400 MHz, Navarro et al. 1995) for PSR J0218+4232. We showed above that this X-ray emission might be extended with angular scale of $\sim 14''$. Navarro et al. (1995) noted that it is possible that the observed unpulsed emission in the radio comes from a compact nebula close to the pulsar. This nebula would then have the same steep spectral index as the pulsed emission and the nebula would have to be smaller than the VLA beam size of $16''$. The latter constraint is consistent with the possible extent found here in X-rays. Navarro et al. (1995) preferred the explanation for which the unpulsed emission comes from the pulsar, however, given our results above, we prefer now the explanation that the unpulsed X-ray and radio emissions are both manifestations of a compact nebula around the pulsar.

Danner et al. (1997) report the detection of an extended source next to PSR B1821-24. The shape of this source is "identical" to the distribution shown in Fig. 1, with the same angular extent. Since the estimated distances are comparable, even the absolute extent is similar, $\sim$0.4 pc. The main difference is that Danner et al. (1997) determine a separation between the pulsar and the extended source of $9''3$. PSR B1821-24 is located near the edge of the globular cluster M28. Since the extended source

appeared to be only slightly offset from the centre of the cluster, Danner et al. (1997) preferred an interpretation as a collection of low-luminosity accreting X-ray binaries in the cluster, over the interpretation as a synchrotron nebula. They considered the synchrotron nebula to be powered by a recent (of the order of 200 years ago) outburst of an unknown source, inconsistent with the pulsar age. However, if the pulsar is powering the nebula it is doing this continuously and no outburst is required. Therefore the interpretation as a synchrotron nebula remains a viable option. The binary ms-pulsar PSR J0218+4232 is not located in a globular cluster. Of the two options mentioned above only the interpretation as a synchrotron nebula remains. Kawai & Tamura (1997) searched for diffuse sources in the vicinity of normal radio pulsars using ASCA X-ray data. They found such sources with high probability for many pulsars, leading to the suggestion that they exist universally for all the active pulsars, and that they are powered by the pulsars. The extended sources near PSR B1821-24 and PSR J0218+4232 add two more candidates, now concerning recycled ms-pulsars.

Wei et al. (1996) discuss the production processes of pulsed and unpulsed gamma-ray emission in ms-pulsars using the outer gap model. They assume that the unpulsed gamma-rays come from a compact region, a couple of light cylinder radii from the pulsar rather than from an extended nebula. This unpulsed non-thermal emission (up to TeV energies) is produced in the interaction of the primary electrons/positrons from one gap in-

teracting with the low-energy photons from another gap, which one expects to cross over just beyond the light cylinder. If we assume that the unpulsed X-ray emission measured from PSR J0218+4232 is the low-energy end of the spectrum of this component, rather than from a small nebula, then one would expect the signature of a point source in our maps. This seems not to be the case. Furthermore, the observed and derived parameters of PSR J0218+4232 and PSR B1821-24 are very consistent. Therefore it is unlikely that the first can produce such a strong unpulsed point-like X-ray component at the pulsar position while there is no evidence for such a component for the second.

Wei et al. (1996) produced pulsed and unpulsed spectra showing that at high-energy gamma-rays the unpulsed component becomes particularly important. In our earlier paper (Verbunt et al. 1996) we noted that the EGRET source 2EG J0220+4228 (Thompson et al. 1995) can be the counterpart of PSR J0218+4232, and we found indications for variation at the pulse period, however, consistent with being 100% pulsed. In fact, also PSR B1821-24 is located close to a possible EGRET source (Fierro 1995), but the identification is less certain, since PSR B1821-24 is just outside the 99% location confidence contour.

At high-energy γ-rays progress can be expected from our scheduled 3 weeks CGRO EGRET exposure in summer 1998 aimed at confirming our indications for pulsed emission above 100 MeV from PSR J0218+4232.

As mentioned above, due to the lack of spectral resolving power of the ROSAT HRI we can not perform a spectral analysis for PSR J0218+4232. Spectral information on the pulsed and DC components can only be obtained by long exposures using ASCA, SAX LECS/MECS and the future AXAF and XMM X-ray observatories.

References

Backer D.C., Sallmen S., 1997, AJ 114, 1539
Becker W., Trümper J., 1993, Nat 365, 528
Becker W., Trümper J., 1997, A&A 326, 682
Buccheri R., Bennett K., Bignami G., et al., 1983, A&A 128, 245
Danner R., Kulkarni S.R., Thorsett S.E., 1994, ApJ 436, L153
Danner R., Kulkarni S.R., Saito Y., Kawai N., 1997, Nat 388, 751
David L.P., Harnden F.R., Kearns K.E., et al., 1997, The ROSAT High Resolution Imager (HRI) Calibration Report, U.S. ROSAT Science Data Center/SAO (http://hea-www.harvard.edu/rosat/rsdc_www/HRI_CAL_REPORT/hri.html)
Daugherty J.K, Harding A.K., 1996, ApJ 458, 278
Fierro J.M., 1995, Ph.D. thesis, Stanford University
Foster R. S., Fairhead L., Backer D.C., 1991, ApJ 378, 687
Halpern J.P., Christopher M., Marshall H.L., 1996, ApJ 462, 908
Heiles C., Habing H.J., 1974, A&AS 14, 1
Ho C., 1989, ApJ 342, 396
de Jager O.C., Swanepoel J.W.H., Raubenheimer B.C., 1986, A&A 170, 187
de Jager O.C., Swanepoel J.W.H., Raubenheimer B.C., 1989, A&A 221, 180
Kawai N., Tamura K., 1997, Proc. IAU Coll. 160, 367
Kawai N., Tamura K., Saito Y., 1998, Adv. in Space Research 21, in press
van Kerkwijk M.H., Proc. IAU Coll. 160, 489
Navarro J., de Bruyn A.G., Frail D.A., Kulkarni S.R., Lyne A.G., 1995, ApJ 455, L55
Rees R.F., Cudworth K.M., 1991, AJ 102, 152
Romani R.W., 1996, ApJ 470, 469
Rots A.H., Jahoda K., Macomb D.J., et al., 1998, ApJ submitted
Saito Y., Kawai N., Kamae T., et al., 1997, ApL 477, L37
Sturner S.J., Dermer C.D., Michel F.C., 1995, ApJ 445, 736
Swanepoel J.W.H., de Beer C.F., Loots H., 1996, ApJ 467, 261
Taylor J.H., Manchester R.N., Lyne A.G., 1993, ApJS 88, 529
Thompson D.J., Bertsch D.L., Dingus B.L., et al., 1995 , ApJS 101, 259
Verbunt F., Kuiper L., Belloni T., et al., 1996, A&A 311, L9
Wei D.M., Cheng K.S., Lu T., 1996, ApJ 468, 207
Zimmermann U., Becker W., Belloni T., et al., 1997, EXSAS User's guide, MPE Report